RESEARCH ARTICLE

Effects of different substrates on nitrogen and phosphorus removal in horizontal subsurface flow constructed wetlands

Rui Xu [1,2,3] · Yong Zhang [1,2,3] · Rong Liu [1,2,3] · Yun Cao [1,2,3] · Guoxiang Wang [1,2,3] · Lingchen Ji [1,2,3] · Yifan Xu [1,2,3]

Abstract

This study aimed to explore the nitrogen and phosphorus removal performance of the horizontal submerged constructed wetland (HSCW) with Ti-bearing blast furnace slag (T). Another two HSCWs, with the converter steelmaking slag (G) and the stone (S) as wetland substrates, respectively, were simultaneously running as control. The results showed that the nitrogen and phosphorus removal capacities of the T-HSCW were generally better than those of another two HSCWs. When the hydraulic retention time (HRT) was 6 days, the effluent concentrations of ammonia nitrogen (NH_4^+-N) and total nitrogen (TN) were 6.66 mg L^{-1} and 14.02 mg L^{-1}, respectively, and the removal rates of NH_4^+-N and TN reached 77.54% and 71.07%, respectively. The T-HSCW had better removal efficiency of phosphorus. The effluent concentration of total phosphorus (TP) was lower than 0.3 mg L^{-1}, and the maximum removal rate could reach 98%. Through the characterization of the three substrates before and after experiments, it was found that the removal of nitrogen and phosphorus by T and G mainly relied on chemical adsorption, while S mainly relied on physical adsorption. Ti could also promote the absorption of nitrogen by plants and increase the nitrogen removal capacity of T-HSCWs.

Keywords Ti-bearing blast furnace slag · Substrate · Horizontal subsurface flow constructed wetland · Adsorption · Nitrogen and phosphorus removal

Introduction

The sewage treatment technology of constructed wetland has been widely used in recent years due to its low construction and operation costs, simple equipment operation, excellent effluent quality, and low energy consumption. Substrates in constructed wetlands, known as filter material and carrier, played an important role in the removal of nitrogen and phosphorus which are the main cause of eutrophication.

✉ Rong Liu
liurongnjnu@yeah.net

1   School of Environment, Nanjing Normal University,
    Nanjing 210023, China

2   Jiangsu Provincial Key Laboratory of Materials Cycling and
    Pollution Controlling, Nanjing 210023, China

3   Jiangsu Center for Collaborative Innovation in Geographical
    Information Resource Development and Application,
    Nanjing 210023, China

Furthermore, substrates provide carrier for plants to grow in wetlands and provide attachment surface for microorganism (Dordio and Carvalho 2013; Tietz et al. 2007). The physical and chemical properties of substrates, such as redox potential, specific surface area, and rate of water content, may affect the treating efficiency of constructed wetlands. Substrates should be selected reasonably according to the water quality of wastewater and the economic analysis (Albuquerque et al. 2009). Related researches showed that zeolite and steel slag were frequently used as substrates in constructed wetlands (Wang et al. 2014c). Zeolite is mainly composed of $CaCO_3$, which has a strong selective adsorption to NH_4^+-N, and can quickly intercept the NH_4^+-N in wastewater (Gaspard et al. 1983; Koon and Kaufman 1975). However, the constructed wetlands with zeolite as substrate were only used to treat nitrogen-containing wastewater because the removal of TP by zeolite was always poor (Miller et al. 2011; Sakadevan and Bavor 1998). Steel slag is the waste residue produced during steelmaking. It is mainly composed of oxides such as CaO, MgO, Al_2O_3, FeO, Fe_2O_3, and SiO_2. These oxides could react with phosphate to form precipitation, and the average removal rate of TP was as high as 90% (Bowden et al. 2009;

Fig. 1 Schematic diagram of laboratory-scale constructed wetlands
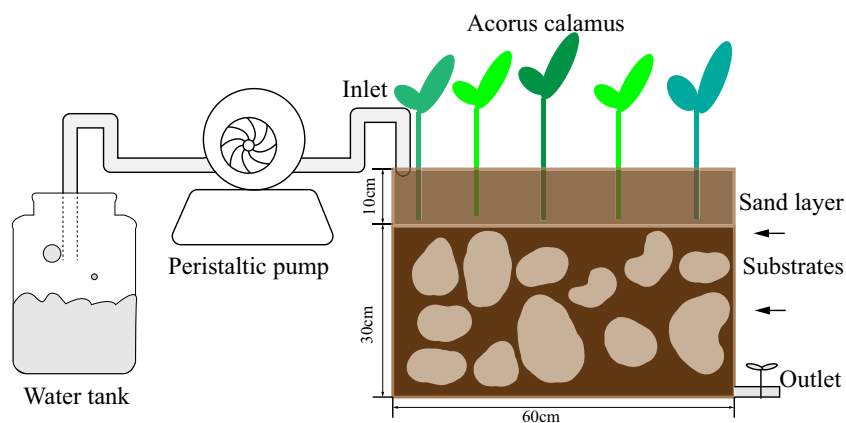
Drizo et al. 2006; Stefanakis et al. 2009; Wu et al. 2011). Nevertheless, the efficiency of nitrogen removal in wastewater via steel slag was poor (Hamdan et al. 2017; Qiu et al. 2014). Because the main component of steel slag was metal oxide, some researchers tried to improve the denitrification ability by chemical modification (Guo et al. 2017; Sui and Zhang 1997), which significantly increased the cost of wastewater treatment. Therefore, new materials were urgently needed to be developed as the substrates of constructed wetlands, giving consideration to simultaneous removal of nitrogen and phosphorus.

Ti-bearing blast furnace slag (T) is a porous metallurgical waste produced when smelting vanadium-titanium magnetite, which contains 20–25% TiO_2 (Yamauchi et al. 2009). The main components of T are CaO, MgO, Al_2O_3, FeO, Fe_2O_3, and SiO_2, which are similar to that of the steel slag, and these components are beneficial for removing phosphorus from the wastewater. Some scholars used T to adsorb the TP in wastewater, and the removal rate could be above 90% (Ma et al. 2009). Besides, some studies showed that the absorption of titanium by plants could promote the growth of roots and increase the activity of various enzymes, especially nitrogenases, which is beneficial to the absorption of nitrogen (Kleiber 2012; Liu et al. 2017).

This study aimed to explore the feasibility of improving the nitrogen and phosphorus removal capacities of wetlands with T as substrate. Slag (G) and the stone (S) were also selected as wetland substrates as control. The mechanisms of nitrogen and phosphorus removal were further analyzed by the Fourier transform infrared spectrometer (FT-IR), the thermogravimetric-differential thermal analyzer (TG-DTA),

and the X-ray fluorescence spectrometer (XRF) methods. This study could provide a reference for the simultaneous removal of nitrogen and phosphorus by constructed wetlands and give a new idea for resource recovery and utilization of Ti-bearing blast furnace slag.

Materials and methods

Experimental setup

Three HSCWs with different substrates were constructed, as shown in Fig. 1. Each HSCW system was consisted of a water tank, a peristaltic pump, and a HSCW. Three HSCWs were named as T-HSCW (with T as substrate), G-HSCW (with G as substrate), and S-HSCW (with S as substrate), respectively. Each HSCW was made of plastics with 40 cm in width, 40 cm in depth, and 60 cm in length and was divided into an influent distribution zone, a main reaction bed, and an effluent collection zone. The main reaction bed of each HSCW was divided into two parts, including an upper sand layer with 10 cm of height and a lower substrate layer with 30 cm of height. The main physical parameters of substrates are shown in Table 1. As can be seen from Table 1, the particle size range, average density, and specific surface area of the three substrates are very similar, thus reducing the impact of physical factors on the experimental results. All HSCWs were planted with *Acorus calamus* according to Pai and Mccarthy (2010). A total of 18 similar-sized plants were planted in three rows in each HSCW. The row spacing between two plants was 10 cm and the column spacing was 6 cm. Each plant was 30~40 cm high and the root depth was 8 cm, approximately.

Wastewater and wetland operation

The experimental wastewater was simulated wastewater containing nitrogen and phosphorus. The concentrations of NH_4^+-N, TN, and TP were 40.07 ± 8.26 mg L^{-1}, 54.2 ± 12.55 mg L^{-1}, and 4.24 ± 0.87 mg L^{-1},

Table 1 The main physical parameters of three substrates

Substrate	T	G	S
Particle size range (mm)	10–20	10–20	10–20
Average density (kg m^{-3})	1770	1690	1940
Specific surface area (m^2 g^{-1})	0.9164	0.8235	1.3824

Fig. 2 Comparison of nitrogen and phosphorus removal efficiencies among the three HSCWs: **a** removal efficiency of NH_4^+-N, **b** removal efficiency of TN, and **c** removal efficiency of TP
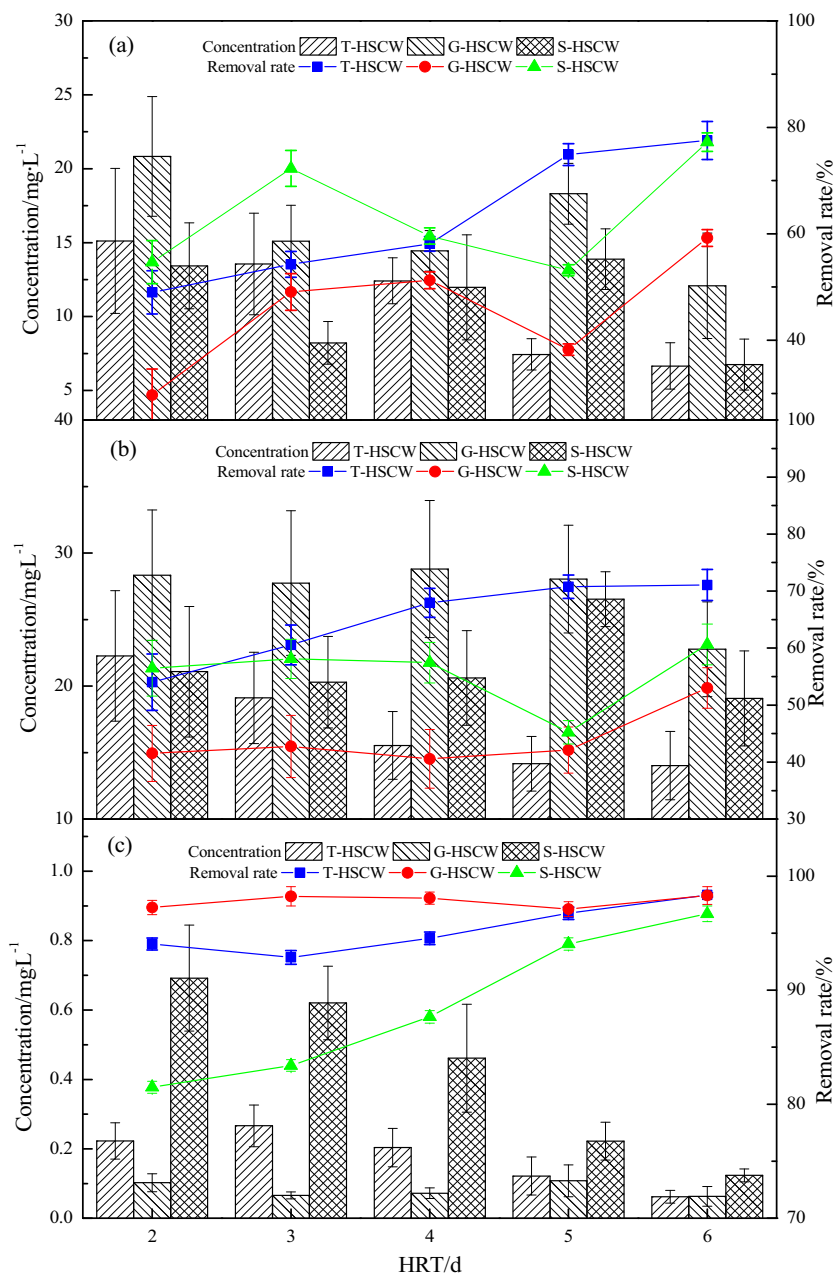
respectively. The pH of the wastewater that ranged from 6.68 to 7.82 was suitable for the survival of most organisms. HSCWs were operated in batch mode. Firstly, the simulated wastewater was discharged into constructed wetlands from the water inlet; secondly, the water intake stopped when constructed wetlands were filled with wastewater, and the reactions were continued for 2–6 days; finally, we drained the wastewater out of the wetland, and HSCWs entered the idle period (1 day). The hydraulic load and the HRT of each HSCW were 0.4 $m^3 \cdot (m^2 \, day)^{-1}$ and 6 days, respectively. The plants grew well in each HSCW during the whole experimental period.

Analytical methods

Water samples were collected from the water tanks and the outlets of the HSCWs every day to monitor water quality and pollutant removal. The concentrations of NH_4^+-N, TN, and TP were measured with salicylic acid-hypochlorite spectrophotometry, potassium persulfate oxidation-UV spectrophotometry, and molybdenum antimony anti-spectrophotometric method, respectively. The pH was recorded with the help of a sensION™ + pH 3 Multi-Parameter Meter. Each experiment was conducted in triplicate. The material characteristics of the three substrates before and after the experiments were further
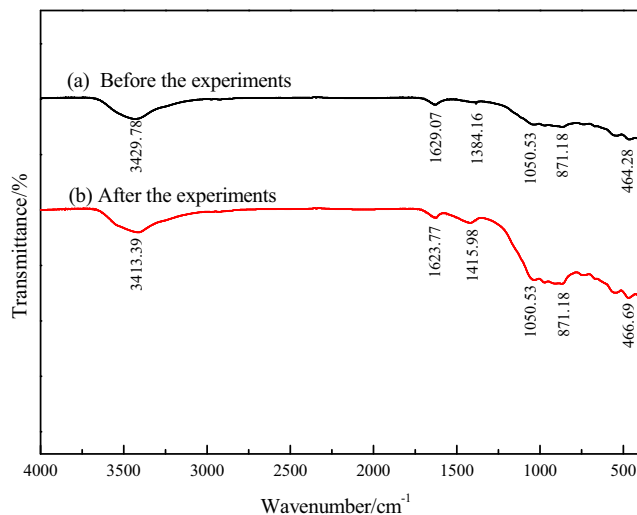
Fig. 3 FT-IR spectra of T before the experiments (**a**) and after the experiments (**b**)

Fig. 4 FT-IR spectra of G before the experiments (**a**) and after the experiments (**b**)

analyzed by FT-IR, TG-DTA, and XRF. FT-IR analysis was used to determine the functional groups by the infrared characteristic absorption bands. TG-DTA analysis was employed to discriminate the components in substrates by changing the quality of the sample with the temperature at constant speed. XRF analysis was used to identify the chemical composition of the sample by X-ray fluorescence spectroscopy.

Results and discussion

Nitrogen and phosphorus removal efficiencies of the three HSCWs

Figure 2 shows the nitrogen and phosphorus removal efficiencies of the three HSCWs during the whole experiments. The denitrification efficiencies of the T-HSCW gradually increased with increasing HRT. When HRT was 6 days, the effluent concentrations of NH_4^+-N and TN were 6.66 mg L^{-1} and 14.02 mg L^{-1}, respectively, and the removal rate of NH_4^+-N and TN was 77.54% and 70.77%, respectively. The nitrogen removal efficiencies of the G-HSCW were poor and instable. The effluent concentrations of NH_4^+-N and TN were 12.08 mg L^{-1} and 22.77 mg L^{-1}, and the removal rates were only 59.23% and 53.02%, respectively. S-HSCW has better nitrogen removal capacity than G-HSCW. The effluent concentrations of NH_4^+-N and TN were 6.75 mg L^{-1} and 19.08 mg L^{-1}, respectively, and the removal rate of NH_4^+-N and TN was 77.22% and 60.63%, respectively. Therefore, we could conclude that T-HSCW had the best denitrification capacity.

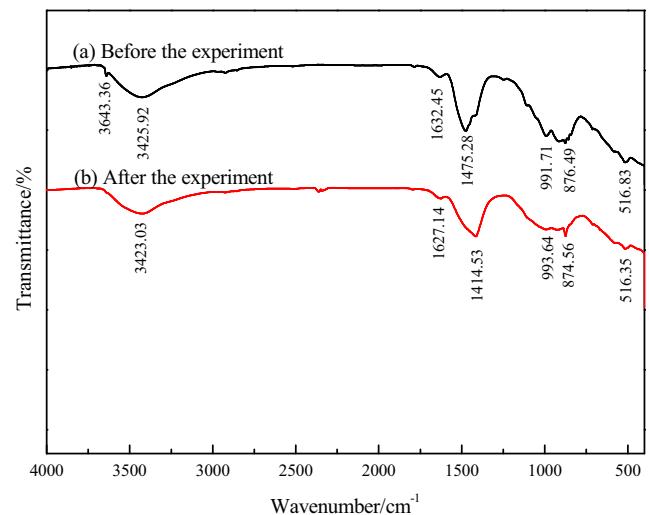The T-HSCW and G-HSCW had notable removal capacities of phosphorus and showed similar tendencies. When HRT was 2 days, the effluent concentrations of TP in this two HSCWs were 0.22 mg L^{-1} and 0.10 mg L^{-1}, and the removal rates were 92.88% and 94.04%, respectively. When HRT was 6 days, both effluent concentrations of TP were 0.06 mg L^{-1} and the removal rates of TP could reach 98%. The removal efficiencies of TP gradually increased with the increasing of HRT in S-HSCW. The effluent concentration of TP was 0.12 mg L^{-1} and the removal rate could reach 96%. Compared to S-HSCW, T-HSCW and G-HSCW had better removal capacities of phosphorus.

In a word, the comparative analysis showed that the T-HSCW had the best comprehensive removal efficiencies of nitrogen and phosphorus in the three HSCWs.
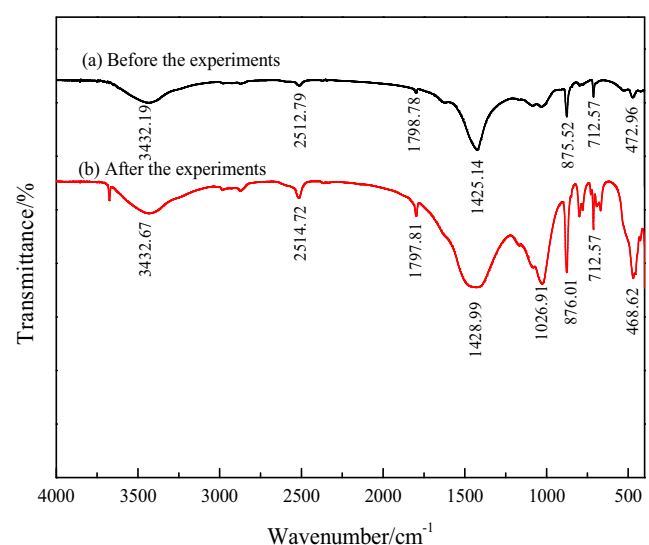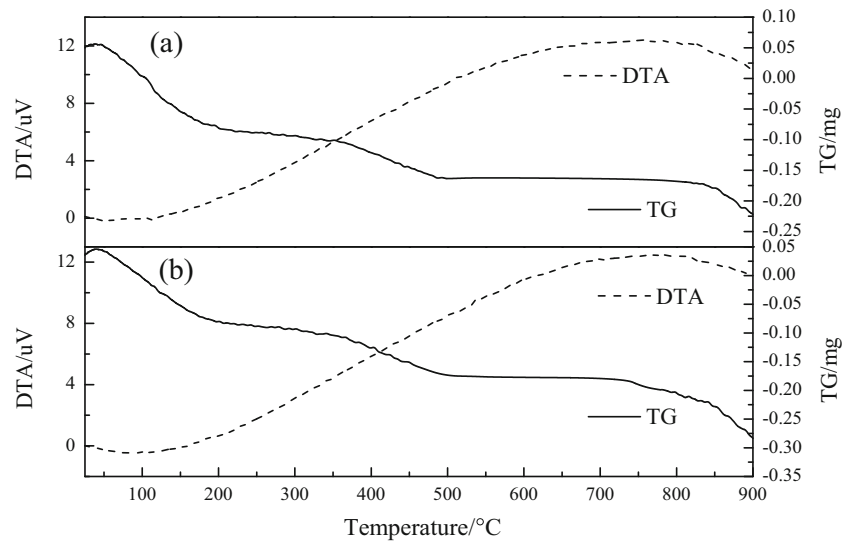

Fig. 5 FT-IR spectra of S before the experiments (**a**) and after the experiments (**b**)

Fig. 6 TG and DTA curves of T before the experiments (**a**) and after the experiments (**b**)

Characterization of the three substrates before and after the experiments

HSCWs with the three different substrates had different degrees of removal rates of nitrogen and phosphorus in wastewater. Thus, FT-IR, TG-DTA, and XRF were employed to characterize the three substrates before and after the experiments to explore the mechanisms of nitrogen and phosphorus removal with the three substrates.

FT-IR analysis

The FT-IR spectrums of T before and after the experiments are shown in Fig. 3. Some absorption peaks in the spectrum indicated the complex components of T. The broad and strong band around 3400 cm^{-1} attributed to O–H stretching vibrations, and the peak at 1630 cm^{-1} was resulted from O–H

flexural vibrations. The band around 1050 cm^{-1} was due to the PO_4^{3-} asymmetric stretching vibrations. The peak around 870 cm^{-1} corresponded to CO_3^{2-} out-of plane bending vibrations. The peak at 465 cm^{-1} was attributed to Si–O–Al flexural vibrations (Mou 2005; Yang et al. 2011; Yang et al. 2015). A weak absorption peak that appeared around 1384 cm^{-1} before the experiments was assigned to NO_3^- (Seyedahmadian et al. 2013), and it disappeared after the experiments, substituted by a weak NH_4^+ stretching vibration peak at 1415 cm^{-1} (Gautier et al. 2010). Besides, the peaks around 1050 and 870 cm^{-1} were stronger after the experiments, because CO_3^{2-} undergone ion exchange reactions with NO_3^- in T and reacted with the metal to produce precipitates. These insoluble matters deposited on the surface of the slag, resulting in the disappearance of NO_3^- absorption peak and the increase of peak value of CO_3^{2-} after the experiments. The appearance of NH_4^+ stretching vibration peak and the increase of peak value

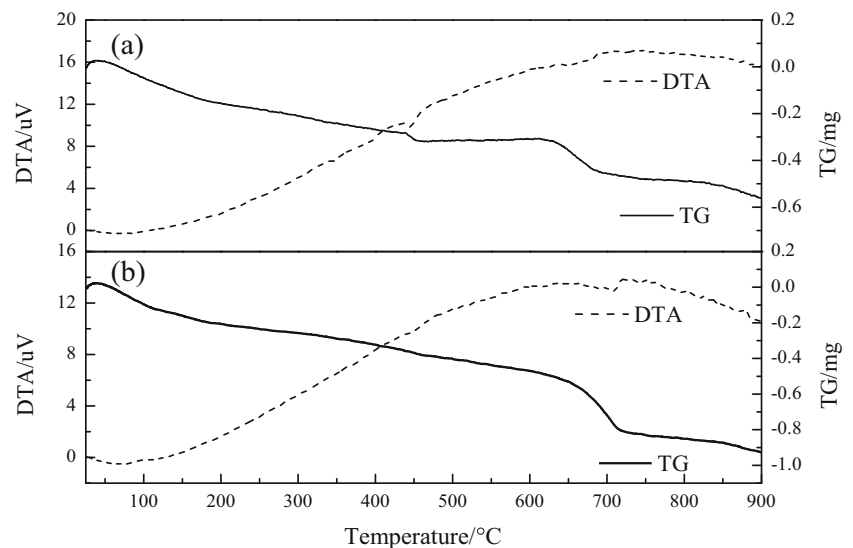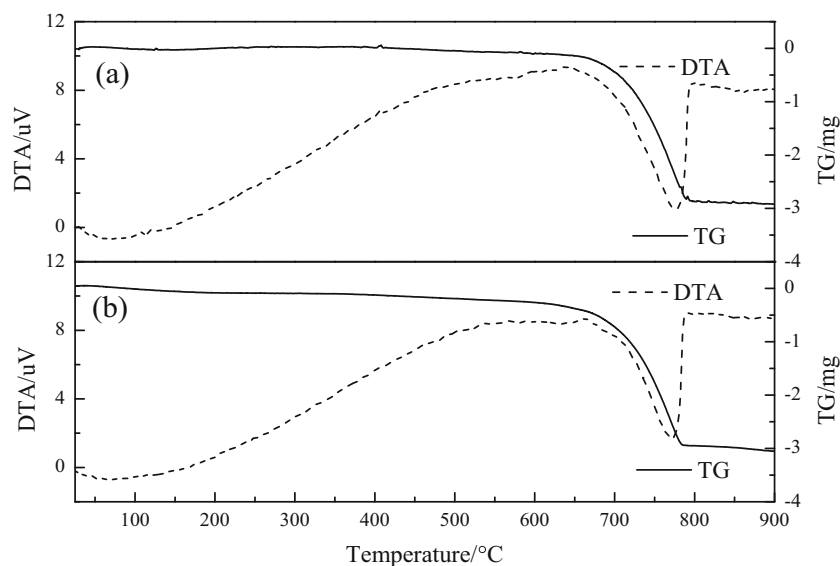Fig. 7 TG and DTA curves of G before the experiments (**a**) and after the experiments (**b**)

Fig. 8 TG and DTA curves of S before the experiments (**a**) and after the experiments (**b**)

of PO_4^{3-} asymmetric stretching vibrations confirmed that NH_4^+ and PO_4^{3-} had been removed by the chemical adsorption process of T.

The FT-IR spectra of G before and after the experiments are shown in Fig. 4. Similar to Fig. 3, the broad and strong band around 3400 cm^{-1} was attributed to O–H stretching vibrations, and the peak at 1630 cm^{-1} was resulted from O–H flexural vibrations. The band around 991 cm^{-1} was due to the Si–OH vibrations. The peak around 875 cm^{-1} corresponded to CO_3^{2-} out-of plane bending vibrations. The peak at 516 cm^{-1} was attributed to Si–O vibrations (Mihailova et al. 2015). The band of Ca–O and N–H was at around 1475 cm^{-1} (Liu 2011) and 1415 cm^{-1} (Wang et al. 2014a, b), respectively. After the experiments, the characteristic peak intensity of Ca–O weakened, indicating that the calcium content in G decreased (consistent with the XRF results), and the band of Ca–O was red-shifted to 1415 cm^{-1}, indicating that the

Ca^{2+} in G and NH_4^+ in the wastewater undergone the reactions of ion exchange so that NH_4^+ was absorbed on the surface of G, and the wastewater was partially denitrified. The characteristic bands of CaO–H at 3644 cm^{-1} (Liu et al. 2010) disappeared after the experiments, indicating that $Ca(OH)_2$ in G was dissolved, which in turn enhanced the alkalinity of the wastewater. Wastewater was detected a pH of 9 after experiments, which was reported to influence the ability of microorganisms to denitrify (Dixit et al. 2014). Therefore, although both T-HSCW and G-HSCW were denitrified by the action of ion exchange and microorganisms, the strong alkaline environment of G-HSCW greatly affected the denitrification ability of microorganisms that played a major role, resulting in a denitrification effect of G-HSCW in Fig. 2 which was inferior to that of T-HSCW.

The FT-IR spectrums of the S before and after the experiments are shown in Fig. 5. The broad and strong

Table 2 Contents of the main elements in the three substrates before and after the experiments

Main elements	T (before)/%	T (after)/%	G (before)/%	G (after)/%	S (before)/%	S (after)/%
Fe	2.03	1.34	19.00	10.06	0.72	0.71
Mn	0.53	0.37	1.77	1.03	/	/
Ti	7.87	6.70	/	/	/	/
V	0.23	0.23	/	/	/	/
Ca	18.57	17.56	24.34	21.98	28.21	27.21
K	0.5	0.52	0.28	0.35	0.72	0.69
Al	5.15	4.57	1.44	0.81	/	/
Mg	/	/	1.14	3.51	/	/
P	0.04	0.16	1.49	4.56	0.06	0.07
Si	10.58	12.21	5.74	6.97	8.38	9.75
[a] Bal	53.81	54.98	44.34	50.12	60.67	60.25

[a] Bal refers to the atomic number of elements less than 11, typically C, N, O, H

Table 3 The main sub-conclusions of FT-IR, DTA-TG, and XRF between three wetlands

Analytical methods	Substances	Phenomena	Conclusions
FT-IR	T	The peak of CO_3^{2-} (870 cm^{-1}) increased	CO_3^{2-} undergone ion exchange reactions with NO_3^- in T and reacted with the metal to produce precipitates
		The peak of NO_3^- (1384 cm^{-1}) disappeared	
		The peak of PO_4^{3-} (1050 cm^{-1}), NH_4^+ (1415 cm^{-1}) appeared	NH_4^+ and PO_4^{3-} had been removed by the chemical adsorption process
	G	The peak of CaO (1475 cm^{-1}) was red-shifted to 1415 cm^{-1}(N-H)	Ca^{2+} in G and NH_4^+ in the wastewater undergo the reactions of ion exchange
		The peak of $Ca(OH)_2$ (3644 cm^{-1}) disappeared	$Ca(OH)_2$ was dissolved, which in turn enhanced the alkalinity of the wastewater
	S	No chemical bond of new substance	physical adsorption
DTA-TG	T	25–200 °C: weight loss increased	In addition to the removal of the free and bound water phases of G, a little NH_4^+ or NH_3 was decomposed and removed.
	G	25–200 °C: weight loss increased	The same as above
		400–500 °C: weight loss	The decomposition of $Ca(OH)_2$
		600–700 °C: weight loss	The decomposition of $CaSiO_3$
	S	25–200 °C: weight loss decreased	Only free surface water and bound water were removed
		700–800 °C: weight loss	The decomposition of $CaCO_3$
XRF	T	The percentage of P increased from 0.04 to 0.16%	Substrates removed P by chemical adsorption
		The percentage of Ti decreased from 7.87 to 6.70%	Ti was dissolved into the wastewater
	G	The percentage of P increased from 1.49 to 4.56%	Substrates removed P by chemical adsorption
	S	The percentage of P was almost unchanged	Physical adsorption

band around 3400 cm^{-1} attributed to O–H stretching vibrations, the peak around 470 cm^{-1} was resulted from

Si–O–Si flexural vibrations (Yang et al. 2015), and the characteristic adsorption peaks of the $CaCO_3$ were observed in the bands around 2512, 1798, 1425, 875, and 713 cm^{-1} (Mou 2005). According to the FT-IR spectrum of the S, the main component in S was $CaCO_3$. There was a new peak presenting in the spectrum around 1026 cm^{-1} after the experiments, which was the band of bending vibration of Si–OH (Jiang et al. 2014). This new peak confirmed that the water flow brought the sand from the upper layer of the system into the S substrate layer, resulting in the increase of SiO_2 after the experiments. The spectrum of S also showed that there was no chemical bond of new substance after the experiments, suggesting that the removal of nitrogen and phosphorus in water by S was only a simple physical adsorption process.

TG-DTA analysis

Figure 6 depicts the DTA and TG plots of the T samples before and after the experiments. The percentages of weight loss of the T at 25–200 °C before and after the experiments were 1.62% and 1.94%, respectively. It was concluded that free water and bound water were removed from the substrate surface in this temperature range. In addition, there was a small amount of decomposition and removal of NH_4^+-N or NH_3 (Qu et al. 2011), indicating that the T possessed a chemical adsorption function of NH_4^+-N from the water, which was consistent with the results in Fig. 3.

Figure 7 shows the DTA and TG plots of the G before and after the experiments. The percentages of weight loss of G at 25–200 °C were 2.06% and 2.12% before and after the experiments, respectively. This result demonstrated that in addition to the removal of the free and bound water phases of G, a little NH_4^+ or NH_3 was decomposed and removed (Qu et al. 2011), confirming that G had a chemical adsorption ability of NH_4^+-N from wastewater, which agreed with the results in Fig. 4. The weight loss from 400 to 500 °C and from 600 to 700 °C was ascribed to the decomposition of $Ca(OH)_2$ and $CaSiO_3$, respectively (Giergiczny and Giergiczny 1988). However, the content of $Ca(OH)_2$ was decreased and the corresponding endothermic peak disappeared in Fig. 7b because of the dissolution of $Ca(OH)_2$ from the substrate to the wastewater after the experiments.

Figure 8 depicts the DTA and TG plots of the S before and after the experiments. The percentages of weight loss of the S at 25–200 °C before and after the experiments were 0.16% and 0.11%, respectively, indicating that only free surface water and bound water were removed from the substrate surface in this temperature range. The endothermic peak and weight loss from 700 to 800 °C could

Fig. 9 Mechanism of nitrogen removal
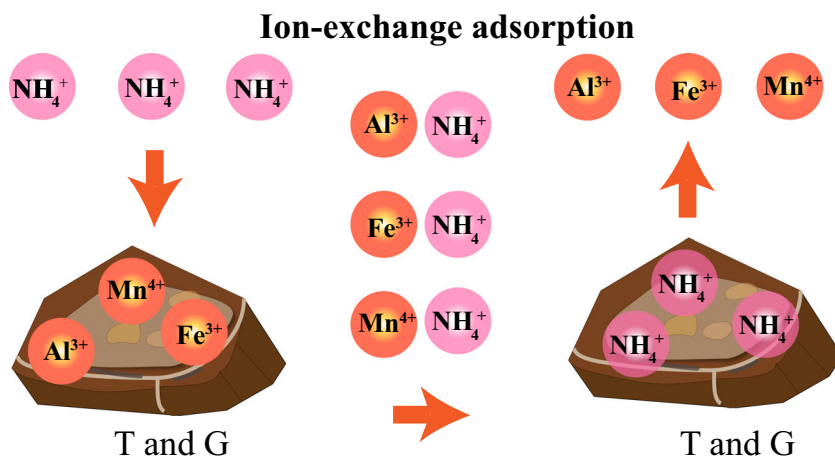
be ascribed to the decomposition of $CaCO_3$ (Donoso et al. 2015), which confirmed that S had only a simple physical adsorption ability to removing NH_4^+-N in wastewater. This result agreed with the results in Fig. 5.
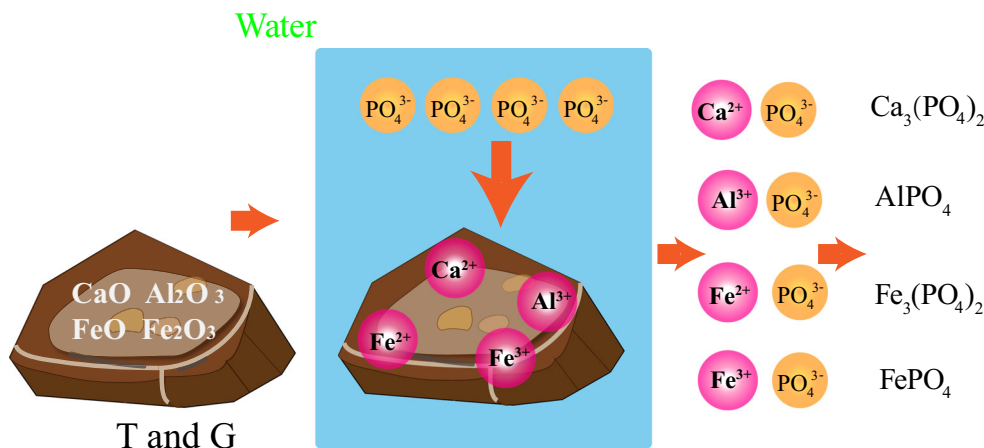
XRF analysis

The XRF results of the three substrates before and after the experiments are shown in Table 2.

It revealed that the relative percentages of the main elements including Ca, Al, Mn, and Fe in T and G declined slightly. However, the percentage of Si increased significantly after the experiments, resulting from the water flowing that made the sand in the top layer of HSCWs spill into the substrates during the experiments. Furthermore, the relative percentage of phosphorus increased from 0.04 to 0.16% and from 1.49 to 4.56% in T and G, which illustrated that the phosphorus removed from the wastewater was accumulated in the substrate layer consisted of T or G. This result confirmed that the substrates of T and G had chemical adsorption abilities to remove phosphorus in

wastewater. The relative percentage of Ti element in the T decreased from 7.87 to 6.70% after the experiments, indicating that Ti was dissolved into the wastewater. The absorption of Ti by plants could promote the growth of roots which were important vegetative organs of plants and promote the absorption of nitrogen and phosphorus from the wastewater by plants (Kleiber 2012; Liu et al. 2017). It was consistent with the results in Fig. 2 that T-HSCW had the best denitrification capacity in the three HSCWs. The relative percentages of rest metals were invariant basically. The main elements in the S were Ca and Si, relatively rare than the other two substrates. After the experiments, the relative percentage of Ca was stable. However, the percentage of Si increased significantly, which was similar to the increasing Si element in T-HSCW and G-HSCW. At the same time, there was no new elements that appeared in the S substrate, which illustrated that the S substrate had only a simple physical adsorption ability of phosphorus from the wastewater.

The results of FT-IR, TG-DTA, and XRF analysis of three different HSCWs are shown in Table 3.

**Fig. 10** Mechanism of phosphorus removal

Mechanism analysis

Mechanism analysis of denitrogenation

Nitrogen removal mechanism of constructed wetlands includes ammonia volatilization, microorganisms' ammonification, nitrification and denitrification, uptake by plants and adsorption by substrates. The nitrification and denitrification of microorganisms were considered to be the main methods of removing nitrogen in constructed wetlands (Bueno et al. 2015), but the adsorption by substrates could not be neglected.

There were some researches that confirmed that the nitrogen removal by mining and metallurgical waste slag mainly depends on the ion-exchange adsorption (Sakadevan and Bavor 1998) between metal ions (e.g., Al^{3+}, Fe^{2+}, and Mn^{4+}) and NH_4^+, and the reaction is as follows:
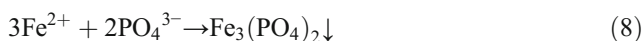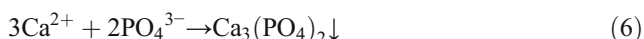
$$Z-M^+ + NH_4^+ \rightarrow Z-NH_4^+ + M^+ \tag{1}$$
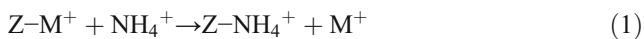
where M^+ represents metal ion and Z means the part of no reaction in mining and metallurgical waste slag (Fig. 9).

According to the characterization results of XRF and FT-IR, S substrate had only a simple physical adsorption ability of NH_4^+-N in wastewater. T and G had chemical adsorption abilities of NH_4^+-N in wastewater due to the decrease of relative percentages of Al, Fe, and Mn and the emerging adsorbed peaks of nitrogenous substance in FT-IR spectrum after the experiments.

Mechanism analysis of phosphorus removal

Some researchers reported that a quantity of free metal oxides concerning Ca, Al, and Fe elements exist in T and G. The reaction between the dissolved metal ions including Ca^{2+}, Al^{3+}, Fe^{3+}, and Fe^{2+} from the substrates and PO_4^{3-} in wastewater takes place and the insoluble precipitate is created (Zhu et al. 2003) (Fig. 10). The reactions are as follows:

$$CaO + H_2O \rightarrow Ca^{2+} + 2OH^- \tag{2}$$

$$Al_2O_3 + 3H_2O \rightarrow 2Al^{3+} + 6OH^- \tag{3}$$

$$FeO + H_2O \rightarrow Fe^{2+} + 2OH^- \tag{4}$$

$$Fe_2O_3 + 3H_2O \rightarrow 2Fe^{3+} + 6OH^- \tag{5}$$

$$3Ca^{2+} + 2PO_4^{3-} \rightarrow Ca_3(PO_4)_2\downarrow \tag{6}$$

$$Al^{3+} + PO_4^{3-} \rightarrow AlPO_4\downarrow \tag{7}$$

$$3Fe^{2+} + 2PO_4^{3-} \rightarrow Fe_3(PO_4)_2\downarrow \tag{8}$$

$$Fe^{3+} + PO_4^{3-} \rightarrow FePO_4\downarrow \tag{9}$$

However, the Ca element in the S was in the form of $CaCO_3$ and that was difficult to dissolve in neutral conditions

(Karageorgiou et al. 2007). Therefore, the main way of phosphorus removal by the S was physical adsorption, which led to a poor phosphorus removal efficiency of S-HSCW.

Conclusions

(1) The T-HSCW had the best comprehensive removal efficiencies of nitrogen and phosphorus in the three HSCWs. The nitrogen removal efficiency of the T-HSCW gradually increased with the extension of HRT. When HRT was 6 days, the effluent concentrations of NH_4^+-N, TN, and TP in wastewater from T-HSCW were 6.66 mg L^{-1}, 14.02 mg L^{-1}, and 0.06 mg L^{-1}, respectively, and the removal rates reached 77.54%, 71.07%, and 98%, respectively.

(2) In addition to the main degradation of nitrogen and phosphorus by microorganisms and plant, we found from the characterization analysis by FT-IR, TG-DTA, and XRF of the three substrates before and after the experiments that S mainly relied on physical interception to remove nitrogen and phosphorus, but T and G removed them mainly by ion exchange. Furthermore, the absorption of Ti dissolved from T by plants could promote the removal of nitrogen from the wastewater.

(3) T-HSCW has good ability to remove nitrogen and phosphorus, confirming the feasibility of T as a substrate in constructed wetlands. It has the function of "treating waste with waste" and provides a new method for the resource utilization of T.

References

Albuquerque A, Oliveira J, Semitela S, Amaral L (2009) Influence of bed media characteristics on ammonia and nitrate removal in shallow horizontal subsurface flow constructed wetland. Bioresour Technol 100:6269–6277

Bowden LI, Jarvis AP, Younger PL, Johnson KL (2009) Phosphorus removal from waste waters using basic oxygen steel slag. Environ Sci Technol 43:2476–2481

Bueno E, Mania D, Frostegard A, Bedmar EJ, Bakken LR, Delgado MJ (2015) Anoxic growth of Ensifer meliloti 1021 by N_2O-reduction, a potential mitigation strategy. Front Microbiol 6:537–547

Dixit S, Dixit A, Kumar P (2014) Nonsurgical treatment of two periapical lesions with calcium hydroxide using two different vehicles. Case Rep Dent 2014:1–4

Donoso MV, Bates F, Montiel J, Huidobro-Toro JP (2015) Modelling the continuous calcination of $CaCO_3$ in a ca-looping system. Chem Eng J 215:174–181

Dordio AV, Carvalho AJP (2013) Organic xenobiotics removal in constructed wetlands, with emphasis on the importance of the support matrix. J Hazard Mater 10:252–253 272–292

Drizo A, Forget C, Chapuis RP, Comeau Y (2006) Phosphorus removal by electric arc furnace steel slag and serpentinite. Water Res 40:1547–1554

Gaspard M, Neveu A, Martin G (1983) Utilisation de la clinoptilolite en potabilisation deseaux—elimination de l'ion NH_4^+. Water Res 17:279–288

Gautier M, Muller F, Forestier LL, Beny JM, Guegan R (2010) NH-smectite: characterization, hydration properties and hydro mechanical behavior. Appl Clay Sci 49:247–254

Giergiczny E, Giergiczny Z (1988) Hydration studies on the system pulverized fly ash—ca$(OH)_2$-CaCl$_2$ using DTA and TG. J Therm Anal 33:821–825

Guo ZY, Martucci NJ, Olivas FM, Tako E, Mahler GJ (2017) Titanium dioxide nanoparticle ingestion alters nutrient absorption in an in vitro model of the small intestine. NanoImpact 5:70–82

Hamdan R, Razi MAM, Zulkafli NF (2017) The effect of HLRs on nitrogen removal by using a pilot-scale aerated steel slag system. Matec Web of Conferences:1–6

Jiang FY, Wang XD, Wu DZ (2014) Design and synthesis of magnetic microcapsules based on n -eicosane core and Fe$_3$O$_4$ /SiO$_2$ hybrid shell for dual-functional phase change materials. Appl Energy 134:456–468

Karageorgiou K, Paschalis M, Anastassakis GN (2007) Removal of phosphate species from solution by adsorption onto calcite used as natural adsorbent. J Hazard Mater 139:447–452

Kleiber T (2012) Effect of titanium application on lettuce growth under Mn stress. J Elem 22:329–337

Koon JH, Kaufman WJ (1975) Ammonia removal from municipal wastewaters by ion exchange. J Water Pollut Control Feder 47:448–465

Liu L (2011) Study on wet process of steel slag. Dissertation, Northeast University. (in Chinese)

Liu HW, Dong YH, Wang HY, Liu Y (2010) Ammonium adsorption from aqueous solutions by strawberry leaf powder: equilibrium, kinetics and efficiencys of coexisting ions. Desalination 263:70–75

Liu SH, Wei XY, Chen JJ, Wang C, Wang XM, Pan DM (2017) Titanium as a beneficial element for crop production. Front Plant Sci 8:597–615

Ma XG, Liu JM, Han C (2009) Experiment of titanium-bearing blast furnace slag adsorbing phosphorus in water. J N Univer 9:1286–1290 (in Chinese)

Mihailova B, Gasharova B, Konstantinov L (2015) Influence of non-tetrahedral cations on Si-O vibrations in complex silicates. J Raman Spectrosc 27:829–833

Miller RL, Jensen BJ, Munns BT, Cardon GE (2011) Use of steel slag to remove dissolved phosphorus from lagoon supernatant. Trans Asae Am Soc Agricul Eng 54:191–196

Mou Z (2005) Preparation and characterization of pillared hydrotalcite and its composite oxide catalysts. Dissertation, Shandong University. (in Chinese)

Pai A, Mccarthy B (2010) Suitability of the medicinal plant, *acorus calamus L.*, for wetland restoration. Nat Areas J 30:380–386

Qiu RF, Cheng FQ, Gao R, Li JF (2014) Ammonia nitrogen removal from micro-polluted river by permeable reactive barriers: lab-scale study with steel slag and fly ash brick in combination as reactive media. Desalin Water Treat 52:365–374

Qu HQ, Wu WH, Wu HJ, Xie JX, Xu JZ (2011) Study on the effects of flame retardants on the thermal decomposition of wood by TG–MS. J Therm Anal Calorim 103:935–942

Sakadevan K, Bavor HJ (1998) Phosphate adsorption characteristics of soils, slags and zeolite to be used as substrates in constructed wetland systems. Water Res 32:393–399

Seyedahmadian M, Houshyarazar S, Amirshaghaghi A (2013) Synthesis and characterization of nanosized of spinel LiMn$_2$O$_4$ via sol-gel and freeze drying methods. Bull Kor Chem Soc 34(2):622–628

Stefanakis AI, Akratos CS, Gikas GD, Tsihrintzis VA (2009) Effluent quality improvement of two pilot-scale, horizontal subsurface flow constructed wetlands using natural zeolite (Clinoptilolite). Microporous Mesoporous Mater 124:131–143

Sui ZT, Zhang PX (1997) Selective precipitating behavior of the boron components from the boron stags. Acta Metall Sin 33:943–951

Tietz A, Kirschner A, Langergraber G, Sleytr K, Haberl R (2007) Characterisation of microbial biocoenosis in vertical subsurface flow constructed wetlands. Sci Total Environ 380:163–172

Wang R, Korboulewsky N, Prudent P, Domeizel M, Rolando C, Bonin G (2014a) Feasibility of using an organic substrate in a wetland system treating wastewater sludge: impact of plant species. Bioresour Technol 101:51–57

Wang XG, Lü SY, Gao CM, Xu XB, Zhang XJ, Bai X, Liu MZ, Wu L (2014b) Highly efficient adsorption of ammonium onto palygorskite nanocomposite and evaluation of its recovery as a multifunctional slow-release fertilizer. Chem Eng J 252:404–414

Wang M, Zhao T, Wang G, Zhou J (2014c) Blend films of human hair and cellulose prepared from an ionic liquid. Text Res J 84:1315–1324

Wu JM, He F, Xu D, Wang R, Zhang XL, Xiao ER, Wu ZB (2011) Phosphorus removal by laboratory-scale unvegetated vertical-flow constructed wetland systems using anthracite, steel slag and related blends as substrate. Water Sci Technol 63(11):2719–2724

Yamauchi S, Nagata K, Sato S (2009) Hydrogen absorption of titanium heat exchanger tubes in MSF desalination plants. Zairyo Kankyo 32:311–317

Yang J, Ren J, Jia G, Tao T, Song F (2011) Characterization of modified Hβ zeolite and its application to catalytic modification of methanol gasoline. Petrochem Technol 40:146–150 (in Chinese)

Yang N, Kuang S, Yue Y (2015) Infrared spectra analysis of several common anhydrous carbonate minerals. J Mineral Petrol 35:37–42

Zhu XZ, Cui LH, Wen XL, Tuo X (2003) Removal efficiency of different substrates used in vertical flow constructed wetlands for treating municipal wastewater. J Agro-Environ Sci 22:454–457 (in Chinese)